NMR compared to band structure calculations of the quaternary superconductor $La_3Ni_2B_2N_{3-x}$

Martin W. Pieper*
Institute of Experimentalphysik, Karl-Franzens University, Universittsplatz 5, A-8010 Graz, Austria

Herwig Michor and Tahir Ali
Institute of Solid State Physics, Vienna University of Technology, Wiedner Haupstrasse 8-10, A-1040 Wien, Austria
(Received 24 February 2012; revised manuscript received 2 May 2012; published 11 June 2012)

We measured susceptibility and NMR spectra, spin-lattice, and spin-spin relaxation of ^{11}B and ^{139}La in the quaternary superconductor $La_3Ni_2B_2N_{3-x}$ and compare these experimental results to full potential density functional theory band structure calculations. The electric field gradients (EFGs) at B and La sites clearly show that the N vacancies are restricted to the N(2*b*) sublattice. Temperature-dependent susceptibility, Knight shift, and nuclear spin-lattice relaxation T_1 are successfully described within the Fermi-liquid model. The Hebel-Slichter peak is suppressed in the mixed state and in the presence of paramagnetic impurities.

DOI: 10.1103/PhysRevB.85.214510 PACS number(s): 76.60.−k, 31.15.A−, 74.25.nj

I. INTRODUCTION

Quaternary superconductors with PbO-type NiB layers as a common structure building element attracted considerable interest in the wake of the high-T_c cuprates. The first members of this family of superconductors with transition temperatures up to 16 K were RNi$_2$B$_2$C (R = Rare Earth and Y)[1] and $La_3Ni_2B_2N_{3-x}$.[2] More recently, the extended family of materials with PbO-type layers gained large attention with the discovery of high-temperature superconductivity in Fe-pnictides and Fe-tellurides (see, e.g., Ref. 3). As compared to other superconductors of this family, relatively few experimental studies have been devoted to the nitride $La_3Ni_2B_2N_{3-x}$ because of its challenging preparation.[4–6] A new route to prepare essentially single phase material used for the present investigation has been reported recently.[7,8] Early investigations of YNi$_2$B$_2$C favored the existence of antiferromagnetic (AF) fluctuations similar to the ones present in the high-T_c cuprates.[9–11] Later work of Suh *et al.* on a single crystal, however, concluded that the susceptibility as well as the NMR data can be understood within straightforward Fermi-liquid theory with only small correlation energies.[12]

We report in this work that the same is true for $La_3Ni_2B_2N_{3-x}$ by computing the band structure within full potential density functional theory (DFT) using the Wien2k code,[13] and comparing the resulting Pauli susceptibility to the experimental susceptibility, and the electric field gradients (EFGs) at ^{11}B and ^{139}La to the ones observed by NMR. We discuss the Knight shift and spin-lattice relaxation (T_1) data above T_c, and briefly comment on the absence of the Hebel-Slichter peak at the transition to the superconducting state as a result of spin diffusion in the presence of Rare-Earth (RE) impurities.

II. DFT AND ELECTRIC FIELD GRADIENTS

$La_3Ni_2B_2N_{3-x}$ crystallizes in the space group $I4/mmm$ (No. 139) with one formula unit per primitive unit cell. The structure may be visualized as NiB layers with Ni in 4*d* and B in 4*e* positions separated by LaN (or RC). Figure 1 shows that there are three LaN layers between NiB in $La_3Ni_2B_2N_{3-x}$, leading to two different positions for La (2*a*, 4*e*) and N (2*b*, 4*e*) each. The central layer is absent in YNi$_2$B$_2$C. Our attempts to influence the carrier concentration by adjusting the number of nitrogen vacancies in this layer revealed a rather narrow range (x = 0.06–0.1) for the variation of the nitrogen stoichiometry in $La_3Ni_2B_2N_{3-x}$.[14]

Polycrystalline samples were grown following the procedure described elsewhere.[7,8] The samples were ground into powders, the structure reported by Huang and co-workers[4] was confirmed for our samples by x-ray diffraction with ion positions given in Fig. 1. The fourfold axis ensures a vanishing asymmetry parameter η of the EFG at all positions in a perfect structure.

For band structure calculations we used full potential density functional theory implemented in the Wien2k program package with the generalized gradient approximation functional of Perdew *et al.* for the exchange potential.[15,16] Convergence criteria for self-consistency were energy, charge, and the electric field gradients at B and La, which we compare to the experimental data below. Note that DFT is a completely different approach to calculating the EFG from first principles than via charge distributions and Sternheimer (anti)shielding factors from induced electric field gradients. The states of all electrons in the Coulomb and exchange potential consistent with the lattice symmetry are calculated self-consistently. The EFG is derived from the resulting charge distribution.[17] Relaxing the atomic positions in the structural model within the DFT calculation moves the atoms in 4*e* positions only by about 1% or less (La to 0.37073, B to 0.19650, N to 0.12578).

The NMR powder spectra shown in Fig. 2 together with the simulated powder spectra for the electric field gradient tensors calculated for ^{11}B ($^{11}I = 3/2, ^{11}\gamma/2\pi = 13.660$ MHz/T, $^{11}Q = 0.04$ barn) and ^{139}La ($^{139}I = 7/2, ^{139}\gamma/2\pi = 6.0146$ MHz/T, $^{139}Q = 0.2$ barn)[18] by DFT indicate that the electronic structure calculated in this way without Ni on-site Hubbard correction or spin-orbit interaction is already close to the experimental one.

The NMR spectra clearly confirm the observation from neutron diffraction that nitrogen vacancies are present in the N(2*b*) positions of the central LaN layer but not in the layer adjacent to NiB.[4] The EFG at ^{11}B, which is neighboring N(4*e*) but is shielded from N(2*b*) by the LaN layer in between is very

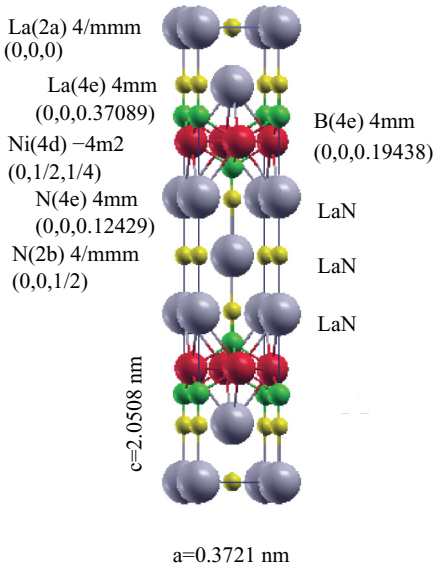

FIG. 1. (Color online) Crystallographic structure of $La_3Ni_2B_2N_{3-x}$ with atom positions in the *I*4/*mmm* space group, multiplicities, and point symmetries.

homogeneous with $\eta = 0$. The observed quadrupole splitting corresponds to $V_{zz} = \pm 1.67 \times 10^{21}$ V/m^2 (the sign cannot be determined by NMR). Comparison with $V_{zz} = -1.64 \times 10^{21}$ V/m^2 calculated for the perfect structure clearly shows that the negative sign is the correct one. For the La spectra, on the other hand, broadening from structural inhomogeneities is evident with all six satellite lines folded into one broad nearly Gaussian line at the same position as the central line.

We utilized two possibilities to approximately treat the nitrogen vacancies within our band structure calculations. Since the EFG at the B sites is experimentally homogeneous throughout the sample, the virtual crystal approximation should be sufficient to estimate the influence of the vacancies on the electronic structure of the NiB layer tested by the EFG at the B site. In our calculations with effective nuclear charges for N(2*b*) down to $Z = 6.4$ (corresponding to $x = 1 - 6.4/7 = 0.09$, consistent with neutron diffraction[14]) the absolute value of the calculated EFG increased only slightly to $V_{zz} = -1.69 \times 10^{21}$ V/m^2 which is slightly smaller than the experimental value but well within any reasonable errors. The weak dependence of the EFG on this doping is another indication for the absence of charge transfer into the NiB layer.

The virtual crystal approximation keeps the perfect crystal symmetry and is, therefore, clearly not suited to treat the influence of the nitrogen vacancies within the LaN layers tested by the EFG at the La sites. The simulated spectra (lines in Fig. 2) show the La-2*a* and La-4*e* powder spectra calculated from $V_{zz} = 6.50 \times 10^{21}$ V/m^2 and $V_{zz} = 2.85 \times 10^{21}$ V/m^2 determined by DFT for the structure without N vacancies. They show the characteristic satellite peaks for $\eta = 0$ which are absent in the experimental spectrum, but the order of magnitude of the calculated V_{zz} clearly is correct. Already the simulation with V_{zz} fixed at the calculated value for La-4*e* and assuming a distribution of asymmetry parameters up to $\eta = 0.5$ provides a reasonable description of the La spectrum (dotted line). Such a distribution is in accord with La EFGs

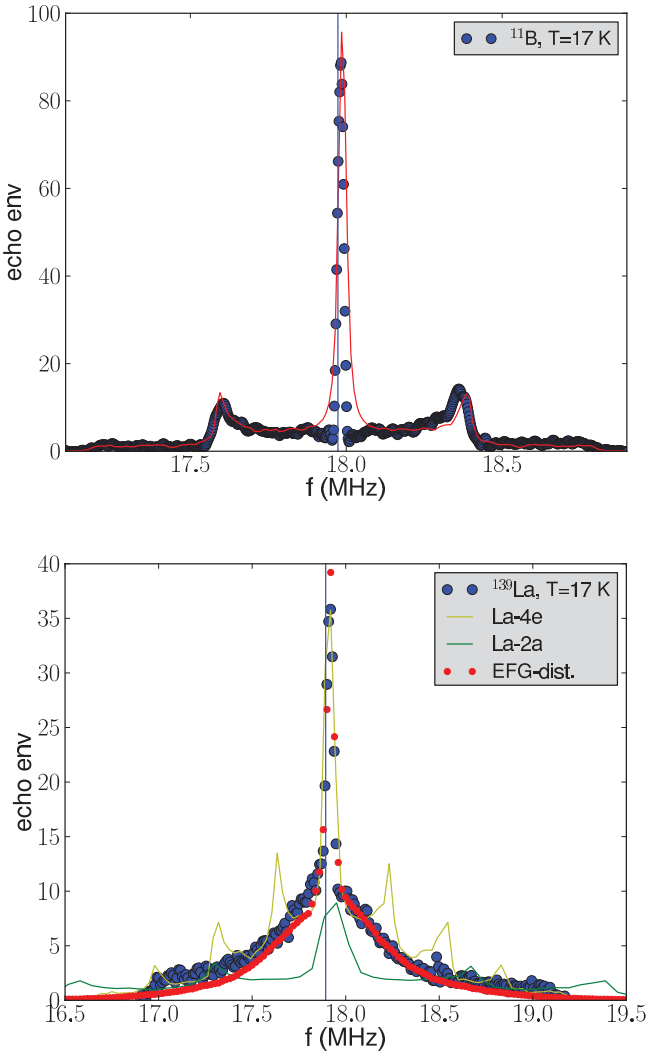

FIG. 2. (Color online) NMR spin echo Fourier transform envelope powder spectra (symbols) of ^{11}B and ^{139}La in $La_3Ni_2B_2N_{3-x}$ at $T = 17$ K. The lines are simulated spectra with parameters calculated by DFT (see text).

taken from a DFT calculation of a small 2×2 supercell in *a* and *b* directions centered at a nitrogen vacancy. Unfortunately, structural relaxation of this supercell and larger supercells are not practicable on the standard PC we used for these computations. There are eight different La positions in this supercell. The influence of a nitrogen vacancy on the EFG at the five of them not neighboring the vacancy is rather small. However, it leads to sizable asymmetry parameters $\eta = 0.2$ and 0.5 for the two La neighbors where this becomes allowed by point symmetry, and it increases the size of the main component of the EFG by more than a factor of 3 at its two nearest La neighbors. The calculation confirms the experimental finding that the EFGs at the more distant B sites are only slightly affected (below 10%) by the nitrogen vacancies.

Electronic correlation effects may be estimated from DFT by including an on-site effective correlation potential[19] $U_{\text{eff}} = U - J$, which we introduced for the Ni 3*d* electrons in the structure model without vacancies. Increasing values of U_{eff}

increase the absolute value of the calculated EFG at the B site. Comparing the values with the experimental one we find $U_{\text{eff}} < 2.0$ eV. When we take into account the influence of the N vacancies discussed above a value $U_{\text{eff}} \approx 1.0$ eV describes our EFG data best. We note that this value is significantly smaller than, for example, $U_{\text{eff}} \approx 5.4$ eV for NiO.

III. SUSCEPTIBILITY AND DFT

We calculated the Pauli susceptibility corresponding to the DFT results discussed above. Figure 3 shows that the calculated density of states $N(\varepsilon)$ near the Fermi energy ε_F for $La_3Ni_2B_2N_{3-x}$ in the perfect structure without nitrogen vacancies is the same as reported in earlier band structure calculations.[20,21] It is seen that the Fermi energy is in the center between Ni valence bands near -2 eV and empty La conduction bands at approximately 3 eV. Four bands cross

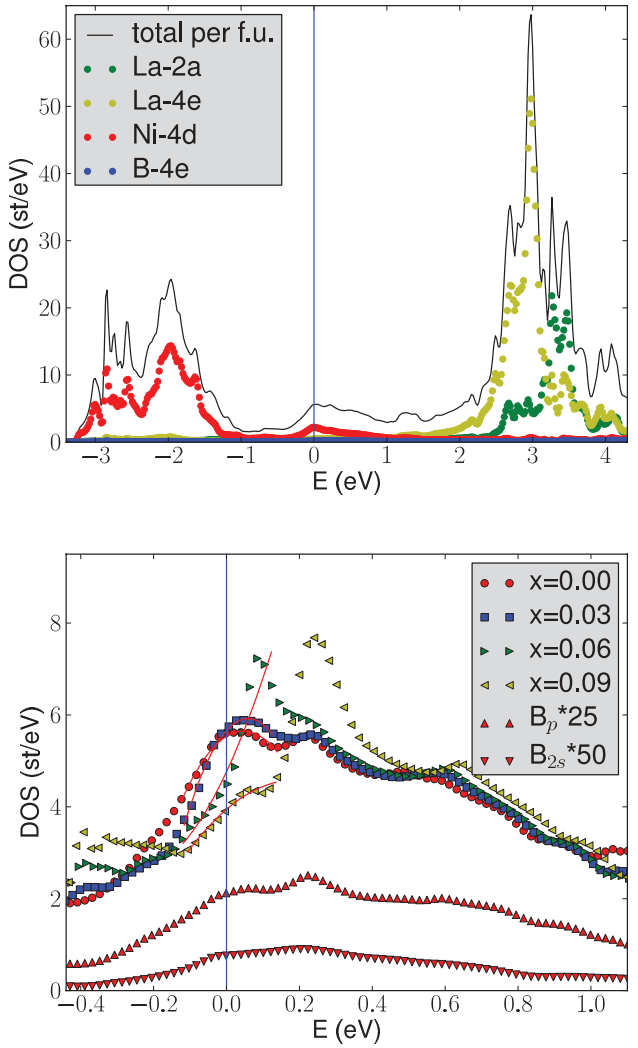

FIG. 3. (Color online) Density of states of $La_3Ni_2B_2N_{3-x}$, $x = 0.0$, from DFT with total La, Ni, and (small) B contributions. The second panel shows the dependency of the total DOS near $\varepsilon_F = 0$ on the N vacancy concentration in the virtual crystal approximation with quadratic fits (lines). The enhanced B-2s and B-p partial DOS for $x = 0$ is also shown.

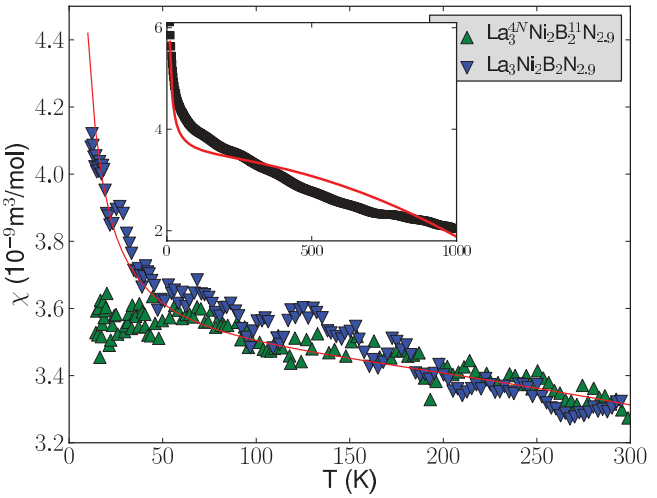

FIG. 4. (Color online) dc susceptibility of $La_3Ni_2B_2N_{3-x}$ in the normal state measured at 5.85 T in a SQUID magnetometer (Δ: 4N-pure La and isotope pure ^{11}B precursors, ∇: NMR sample prepared from commercial precursors). Inset: dc susceptibility of a different sample measured up to 1000 K in a Quantum Design PPMS vibrating sample magnetometer (commercial precursors). The red lines are calculated from Eq. (1) with parameters from DFT (see text).

ε_F where a maximum in the density of states is situated originating from a Ni d band which sits on top of a broad band of mostly La($4e$) character and contains a small amount of B_{2s} and B_p states. Introducing N vacancies within virtual crystal approximation shifts ε_F at small concentrations to the low energy side of this maximum without affecting the overall band structure. At higher defect concentrations, however, a narrow peak from La($4e$) states just above ε_F shifts to higher energies, changing the shape of $N(\varepsilon)$ at the Fermi energy significantly.

In Fig. 4 we compare the temperature dependence of the dc susceptibility measured for different samples in a SQUID magnetometer below $T = 300$ K, and in a vibrating sample magnetometer up to $T = 1000$ K. We consider three contributions to $\chi(T)$ with different temperature dependence:

$$\chi(T) = C/T + \chi_0 + \alpha\chi_P(1 - D_E T^2). \qquad (1)$$

From the direct comparison in Fig. 4 between the sample prepared with commercial La which was used for NMR because of its well characterized superconducting properties, and the one prepared from high purity (4N) La by Ames MPC[22] the first (Curie) contribution can be assigned to Rare-Earth moments from impurities on the La sublattices. The Curie-constant C of a fit displayed in the figure corresponds to 35 ppm Gd at La sites, similar to values reported elsewhere.[11] This assignment is also consistent with the observation of an increasing NMR linewidth with decreasing temperature in the normal state. Such a temperature dependence of the linewidth is expected from dipolar fields and RKKY interactions with statistically distributed 4f moments.

The second contribution contains the core electron susceptibility and the orbital contributions from van Vleck and itinerant Landau susceptibilities. We are not aware of a reliable way to calculate these susceptibilities in a complex metallic band structure as the present one and assume below only

that they are independent of temperature. Experimentally we observed a large scatter in χ_0 from different samples which we ascribe tentatively to variations in the defect structures connected with the RE impurities and the N vacancies. These defect contributions are compensated in the figure by adding a temperature-independent diamagnetic contribution (0.7×10^{-3} [10^{-6} m^3/mol]) to the data for the sample prepared with commercial precursors.

The third contribution is the (molar) free conduction electron spin Pauli susceptibility $\chi_P = \mu_0 N_A \mu_B^2 N(\varepsilon_F)$. The T^2 term with $D_E = \frac{(\pi k_B)^2}{6}\{[N'(\varepsilon_F)/N(\varepsilon_F)]^2 - N''(\varepsilon_F)/N(\varepsilon_F)\}$ with slope $N'(\varepsilon_F)$ and curvature $N''(\varepsilon_F)$ of the total density of states at the Fermi energy accounts for the softening of the Fermi function with increasing temperatures.[23] The (Stoner) enhancement factor α accounts for electron correlation effects.

The line is the result from a fit to the impurity contribution at low temperature, $\chi_P = 2.30 \times 10^{-3}$ [10^{-6} m^3/mol] and $D_E = 3.57 \times 10^{-7}$ [K^{-2}] calculated from the DFT band structure (in the case $x = 0.03$ shown in Fig. 4), and a Stoner enhancement $\alpha = 1/(1 - U/W) \approx 1.9$ estimated from the calculated bandwidths $W \approx 2.2$ eV and $U_{\text{eff}} \approx 1.0$ eV discussed above. With these rather crude assumptions the resulting susceptibilities for $x = 0.0$ and $x = 0.03$ agree remarkably well with the experimental one if the temperature-independent diamagnetic contribution for the sample prepared from high purity La is $\chi_0 = -0.95 \times 10^{-3}$ [10^{-6} m^3/mol]. We note that this value is close to $\chi_L = -\chi_P/3$, the diamagnetic Landau contribution for quadratic dispersion. At larger x, the bands crossing ε_F do not shift rigidly (compare Fig. 3) and the calculated χ_P does not describe the experimental temperature dependence any more.

In Fig. 5 we show the Knight-shift data for ^{11}B and ^{139}La below 250 K which we compare with the susceptibility. The vertical lines indicate the superconducting transition

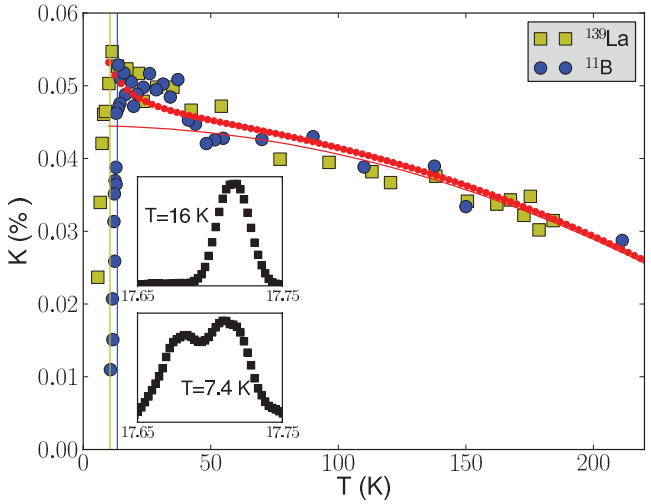

FIG. 5. (Color online) Knight shift of ^{11}B ($B_0 = 1.3$ T, $T_c = 13.4$ K) and ^{139}La (scaled, see text, $B_0 = 3.0$ T, $T_c = 10.5$ K) below 250 K compared to the susceptibility calculated from DFT shown in Fig. 4 according to Eq. (2) with (dotted) and without (line) impurity contribution. The vertical lines indicate the transition temperatures, the insets show that the B-central lines develop a double peak structure in the field cooled mixed state below T_c.

onset temperatures $T_c(1.3T) = 13.4$ K and $T_c(3.0T) = 10.5$ K determined by the onset of the diamagnetic shift from the superconducting phase in our measurements of the ^{11}B and ^{139}La resonance, respectively. These values are in accord with the ones reported elsewhere from susceptibility and specific heat measurements.[24] The upper inset shows that there is a considerable inhomogeneous linewidth of 20 kHz FWHM at $T = 16$ K just above T_c for the ^{11}B resonance. Associated with this inhomogeneous width is the observation of a large $\pi/2 - \pi -$ pulse spin echo which we utilized to measure the spectra. The broadening has been ascribed above to dipolar and RKKY contributions from RE impurities, which increase with decreasing temperature since the expectation value of the RE magnetization increases. An additional, temperature-independent contribution to the linewidth is expected from structural inhomogeneities associated with the presence of the N vacancies. Finally, there are inhomogeneous dipolar fields due to the demagnetizing fields of irregular shaped grains in the overall spherical sample, and possibly a shift due to the noncubic lattice symmetry.[25] A direct comparison of single crystal and powder spectra in the structurally related YNi_2B_2C indicates that the dipolar shift from the noncubic lattice can be neglected, and that on average spherical powder grains can be assumed.[11] A direct calculation of the lattice sum for Gd moments on the La sites in a Lorentz sphere of $La_3Ni_2B_2N_{3-x}$ confirms that the shift due to the noncubic lattice can safely be neglected.

We used ^{11}B isotopic pure element as a reference and corrected for the quadrupole shift of the central transition in a field perpendicular to the main eigenaxis of the EFG calculated by numeric diagonalization of the spin Hamiltonian. No separate reference was measured for ^{139}La, a reference frequency $^{139}f_{\text{ref}}$ calculated from the different γ and nominal fields leads to $^{139}K(T = 16\text{ K}) = 0.11\%$, a factor of 2 higher than the values shown in Fig. 5. The data in the figure are obtained by adjusting $^{139}f_{\text{ref}}$ so that they coincide with ^{11}K to show that the temperature dependence is the same.

The absolute values and temperature dependence of ^{11}K closely resemble the ones reported for the B resonance in YNi_2B_2C, where several authors observed an increasing Knight shift with decreasing temperature. Our data for the La resonance differ, however, from the ones reported for Y in YNi_2B_2C in that $^{89}K_\perp(T = 16\text{ K}) \approx 0.025\%$ *increases* with increasing temperature. This negative hyperfine coupling has been attributed to an indirect coupling to the d-electron magnetization via polarization of s electrons at the Y site. The Y Knight shift shows a significant anisotropy due to orbital contributions to the susceptibility, which we cannot determine for La because suitable single crystals are not yet available.

In the discussion above we described the susceptibility by an impurity part, a temperature-independent contribution χ_0 summing up core and orbital susceptibilities, and a temperature-dependent Pauli spin susceptibility. If we assume a single hyperfine coupling ^{11}A of the ^{11}B nuclear spin to the spins at the Fermi surface, and furthermore assume that the impurities do not contribute to a line shift, we can write the temperature-dependent shift as

$$^{11}\sigma_{(T)} = \sigma_0 + {}^{11}K_{(T)} = A_0\chi_0 + {}^{11}A\alpha\chi_P(1 - D_E T^2), \qquad (2)$$

with the hyperfine coupling constant A_0 describing the effective coupling to the temperature-independent part of the susceptibility. The line in Fig. 5 shows a fit with the total hyperfine coupling constant $^{11}A = 2.5$ [10^6 mol/m^3] (=17.5 [T/$\mu_B N_A$]) and an offset $\sigma_0 = -1.05 \times 10^{-4}$.

From Eq. (2) it is seen that the hyperfine coupling constant is the ratio of the slope of the Knight shift with temperature to the one of the susceptibility. It turns out that the slope of the Knight shift is surprisingly large, resulting in a large hyperfine coupling constant. Assuming that only B-2s electrons have an appreciable spin density at the B nucleus one expects that the Knight shift is dominated by the hyperfine coupling $^{11}A_{2s}$ to their Pauli spin susceptibility $\chi_{B,2s}$:

$$^{11}K = {}^{11}A_{2s}\chi_{B,2s}. \tag{3}$$

The Pauli spin susceptibility χ_i of any part of the electrons is proportional to their partial density of states $N_i(\varepsilon_F)$, $\chi_i = g\mu_0\mu_B^2 N_i(\varepsilon_F)/4$, so one can substitute (provided the Lande factors g are equal) $\chi_{B,2s} = \chi_P N_{B,2s}(\varepsilon_F)/N(\varepsilon_F)$ by the experimental total Pauli spin susceptibility χ_P and solve for the hyperfine coupling constant:

$$^{11}A_{2s} = \frac{^{11}K}{\chi_P}\frac{N(\varepsilon_F)}{N_{B,2s}(\varepsilon_F)}. \tag{4}$$

With $^{11}K(16\,\mathrm{K}) = 5.6 \times 10^{-4}$ from Fig. 5, $\chi_P = 2.30$ [10^{-9} m^3/mol] in accord with DFT as discussed above, $N(\varepsilon_F) = 5.65$ [states/eV f.u.], $N_{B,2s}(\varepsilon_F) = 0.0152$ [states/eV B], and 2 boron per formula unit (f.u.) we find $^{11}A_{2s} = 40$ [10^6 mol/m^3] (=280 [T/$\mu_B N_A$]). Assuming furthermore that the amplitude of the 2s wave function at the B nucleus in the metal is not very different from the atomic one, we can compare this to the much smaller atomic hyperfine coupling $^{11}A_{2s}^{(\mathrm{at})} = 1000$ [kG/$\mu_B N_A$] = 14.0 [mol B/10^{-6} m^3].[25] A similar discrepancy between the calculated temperature dependence of the susceptibility and the Knight shift in YNi_2B_2C was left unexplained by Suh *et al.*.[12]

The Fermi contact hyperfine coupling constants can be independently found from DFT in a spin resolved calculation by solving the self-consistent field cycle with a fixed spin moment as a boundary condition for the spin distribution or, alternatively, by introducing a magnetic field as an orbital potential within the muffin-tin spheres. We assume that the self-consistent solution is an approximation for the experimental field induced state in both cases. The up and down spin densities in the volume of the B nucleus as well as the resulting Fermi contact hyperfine fields of the valence as well as the core electrons are calculated separately.[26] The distinction between both in the code is that core electrons are well localized within an atomic muffin-tin sphere and efficiently described by atomic wave functions, while valence electrons contribute to the charge distribution outside the atomic muffin-tin sphere and are described by plane waves. For B in $La_3Ni_2B_2N_{3-x}$ only B-1s is treated as core orbital, B-p and B-2s are valence states and both have a small contribution to the DOS at the Fermi energy. The main contribution to the hyperfine field is from valence electrons, the field from core electrons is opposite and six times smaller. The Fermi contact coupling constant of B to the valence spin moments is $^{11}A^{(\mathrm{val})} = 524$ [kG]/[$\mu_B N_A$] = 7.47 [mol B/10^{-6} m^3] independent of the method of the calculation, fixed spin moment, or orbital potential.

This coupling constant to the boron valence electrons compares favorably with the experimental value: Substituting in Eq. (4) $N_{B,2s}(\varepsilon_F)$ by the combined density of states of the boron valence electrons $2N_{B,p+2s}(\varepsilon_F) = 2(0.0849 + 0.0152)$ we get $^{11}A_{p+2s} = 6.8$ [mol B/10^{-6} m^3] (=48 [T/$\mu_B N_A$]) from the experiment.

The parabolic temperature dependence of χ_P fits the nearly linear temperature dependence of the Knight shift not very well. The poor description of the temperature dependence suggests the influence of another temperature-dependent contribution to the susceptibility with a significant hyperfine coupling. No shift is expected from the dipolar fields of randomly distributed Rare-Earth impurities, but this is in general not true for the RKKY interaction, that is, the coupling to the conduction band polarization $\sigma(r)$ induced by magnetic impurities at position $r = 0$. The polarization in a sphere of radius R is proportional to $JS_z\chi_P[1 - \sin(2k_F R)/2k_F R]$, where S_z is the bare moment of the impurity, J is the coupling constant between S and the conduction electron spin, and k_F is the radius of the Fermi sphere. The dotted line in Fig. 5 results in the assumption that the conduction band polarization of neighboring RE ions does not cancel perfectly in this complex band structure and that, therefore, the Curie susceptibility couples indirectly to ^{11}B with the hyperfine coupling constant $^{11}A = 2.5$ [mol B/10^{-6} m^3] we determined from the ratio of the average of the slopes $[dK(T)/dT]/[d\chi(T)/dT]$. Additional work with better control of the impurity concentration is in progress to clarify the situation.

IV. NUCLEAR SPIN RELAXATION

We measured the nuclear spin lattice relaxation rates $1/^{11}T_1$ and $1/^{139}T_1$ on the central transitions of the spectra shown in Fig. 2 in the same field as the Knight shifts. For ^{11}B a single time constant in the standard Master equation[27] describes the relaxation in the four level system ($I = 3/2$) well at temperatures above T_c, but it becomes rapidly worse with the increasing linewidth in the inhomogeneous mixed state below T_c (see insets Fig. 5). This is usually ascribed to the influence of spin diffusion or inhomogeneous excitation and gives rise to a relatively large error in the T_1 data below T_c shown in Fig. 6. In this situation the relaxation can frequently be fitted to the phenomenological $S_{(t)} \propto \exp[-(t/\tau_1)^\beta]$ with a single relaxation time constant τ_1 which replaces the multiexponential decay of the Master equation by a stretched exponential. We find $\beta \approx 0.85$ above T_c, and values down to $\beta = 0.5$ in the mixed state below. The inhomogeneities are larger for the La resonance due to the neighboring N vacancies. In addition, the relaxation behavior is more complex in this $I = 7/2$ system. The fits with a single time constant and a Master equation are, therefore, less reliable than for the B resonance, but due to the different nuclear spin they still allow a better comparison of the resulting time constants for ^{11}B and ^{139}La than the stretched exponential.

Figure 6 shows that for both isotopes a Korringa relation

$$\frac{1}{^iT_1} = C_K T \alpha_K (^i\gamma\, ^iK_{(T)})^2 \tag{5}$$

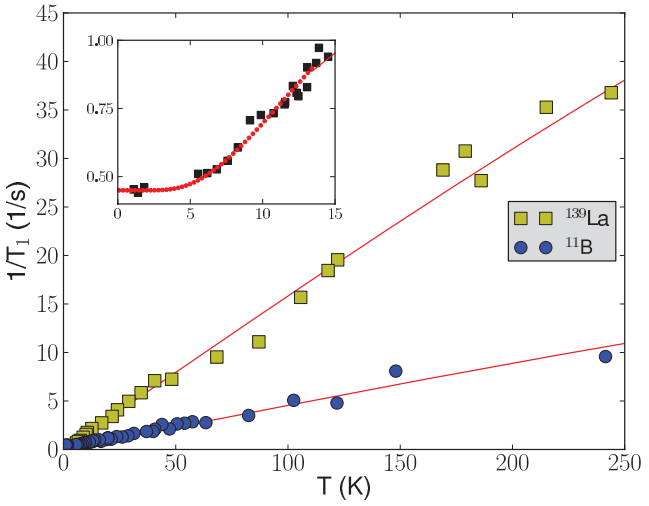

FIG. 6. (Color online) Nuclear spin lattice relaxation rate of ^{11}B and ^{139}La with fits (lines) to a Korringa law with a temperature-dependent Knight shift calculated from Eq. (2). The inset shows the low temperature regime for ^{11}B with the Korringa law above $T_c = 13.4$ K (line) and the exponential expected from BCS theory below (dotted).

holds, where $C_K = (hk_B)/(\mu_0\mu_B)^2$ is the Korringa constant for free electrons, ${}^i\gamma$ is the gyromagnetic constant of isotope $i = 11(\mathrm{B}), 139(\mathrm{La})$, ${}^iK_{(T)} = {}^iA\chi_{P(T)}$ is the also isotope specific, slightly temperature-dependent Knight shift from the Pauli spin susceptibility without Stoner enhancement as discussed above, and α_K is a correction to account for electronic correlations.[28]

For the boron resonance we insert the experimental ${}^{11}A = 2.5$ [10^6 mol/m^3] from above and find $\alpha_K = 0.11$. The free electron relaxation rate calculated with the Korringa relation is, therefore, significantly larger than the experimental one. Such a suppression of transverse fluctuations by electronic correlations is a common observation in transition metal systems. The factor of 8 we find here is, however, rather large and could indicate some additional mechanism suppressing the fluctuations. The relaxation rate of La is larger than the one of B, showing that the smaller ${}^{139}\gamma$ is overcompensated by a stronger hyperfine coupling. In view of the strong influence of the N vacancies we observed for the EFG at the La sites we made no attempt to calculate ${}^{139}A$ within DFT and only note that within the virtual crystal approximation we found both positive and negative ${}^{139}A$, depending on site, spin orbit coupling, and the presence of a Hubbard potential U. Since α_K is a property of the electronic system we can estimate ${}^{139}A = 11$ [10^6 mol/m^3] ($= 77$ [T/$\mu_B N_A$]) from the Korringa relation observed for the La resonance.

Figure 6 shows that in the field cooled mixed superconducting state below $T_c = 13.4$ K (see Fig. 5) $1/T_1$ of B (as well as La, not shown) drops without a Hebel-Slichter peak. This behavior has been reported for other quaternary NiB superconductors as well[9,10,12] and is ascribed to nuclear spin diffusion in the presence of a flux line lattice and Rare-Earth impurities. The temperature dependence can be described by[29]

$$\frac{1}{T_1} = W_0 + ae^{-\Delta/T}, \tag{6}$$

where we fixed Δ to its BCS value $2\Delta = 3.52T_c$, set $W_0 = 0.45$ [1/s] in accordance with the offset observed in a free linear fit to $1/T_{1,B}$ above T_c, and fitted only the amplitude $a = 2.6$ [1/s].

The presence of a spin diffusion contribution even in the normal state above T_c can also be inferred from the difference between the spin-spin relaxation time T_{2H} as observed in the decay of a conventional Hahn echo, and the exponential decay constant $T_{2\mathrm{CP}}$ of the signal in a Carr-Purcell $\pm\pi$-pulse train.[30] For the Hahn echo we find $T_{2H} = 680$ [μs] while $T_{2\mathrm{CP}} = 1100$ [μs] is significantly longer, as expected in the presence of spin diffusion which is partly suppressed in a multipulse sequence. $T_{2H} < T_{2\mathrm{CP}}$ is observed below as well as above T_c indicating that spin diffusion does not occur towards vortex cores but due to RE impurities. We note that $1/T_2$ is, in contrast to $1/T_1$, constant above T_c (at least up to 25 K), and has a maximum below T_c at $T = 11$ K which we ascribe to longitudinal field fluctuations from motions of flux lines which freeze at low temperatures into the static inhomogeneous broadening shown in the lower inset of Fig. 5.

V. CONCLUSION

Susceptibility, NMR spectra, Knight shift, and spin lattice relaxation of ^{11}B and ^{139}La in $La_3Ni_2B_2N_{3-x}$ below room temperature are very similar to the ones in YNi_2B_2C and other closely related NiB-based superconductors. We compare our experimental results to predictions from full potential DFT calculations based on the crystal structure. The electric field gradients are calculated remarkably accurate at least for ^{11}B, allowing us to identify N($2b$) as the site of the nitrogen vacancies in the lattice, and to estimate an effective correlation energy $U_{\mathrm{eff}} \approx 1.0$ [eV] for Ni.

The Pauli spin susceptibility calculated from this band structure and the corresponding Stoner enhancement describes the weakly temperature-dependent experimental susceptibility very well with a temperature-independent diamagnetic susceptibility as the only free parameter. Similar to what has been reported for YNi_2B_2C we find a remarkably strong temperature dependence of the Knight shift which is not compatible with a description by the atomic hyperfine coupling constant from the literature and the calculated band structure. However, the valence electron hyperfine coupling constant calculated within DFT is again fairly close to the (large) experimental one.

The spin-lattice relaxation rate of both ^{11}B and ^{139}La follow a free electron Korringa law. Taking the hyperfine coupling constant of B at face value one finds that the correlation factor indicates a significant suppression of longitudinal fluctuations. We presented evidence from susceptibility and nuclear spin relaxation for the presence of RE impurities and argued that they might be responsible not only for the suppression of these longitudinal fluctuations and of the Hebel-Slichter peak, but also for the remaining discrepancies in the temperature dependence of the Knight shift and the susceptibility. The successful and consistent description of our susceptibility and NMR data with DFT and a rather small on-site effective Hubbard potential U at the Ni sites gives no evidence for any strong electronic correlation effects in these materials.

ACKNOWLEDGMENTS

It is a pleasure to thank the group of K.-H. Schwarz at the TU Vienna for making Wien2k available to us. M.W.P. gratefully acknowledges financial support by the Austrian FWF under Grant P21073-N20. The financial support for research by T.A. was provided by Higher Education Commission, Pakistan.

*pieper@ifp.tuwien.ac.at

[1] R. Cava, H. Takagi, H. Zandbergen, J. Krajewski, W. F. Peck Jr., T. Siegrist, B. Batlogg, R. van Dover, R. Felder, K. Mizuhashi, J. Lee, H. Eisaki, and S. Uchida, Nature (London) **367**, 252 (1994).

[2] R. Cava, H. Zandbergen, B. Batlogg, H. Eisaki, H. Takagi, J. Krajewski, W. F. Peck Jr., E. Gyorgy, and S. Uchida, Nature (London) **372**, 245 (1994).

[3] F. Ronning, E. D. Bauer, T. Park, N. Kurita, T. Klimczuk, R. Movshovich, A. S. Sefat, D. Mandrus, and J. D. Thompson, Physica C **469**, 396 (2009).

[4] B. C. C. Q. Huang, A. Santoro, R. J. Cava, J. J. Krajewski, and W. F. Peck Jr., Physica C **244**, 101 (1995).

[5] H. Michor, R. Krendelsberger, G. Hilscher, E. Bauer, C. Dusek, R. Hauser, L. Naber, D. Werner, P. Rogl, and H. W. Zandbergen, Phys. Rev. B **54**, 9408 (1996).

[6] H. Michor, G. Hilscher, R. Krendelsberger, P. Rogl, and F. Bourée, Phys. Rev. B **58**, 15045 (1998).

[7] T. Ali, C. Rupprecht, R. T. Khan, E. Bauer, G. Hilscher, and H. Michor, J. Phys.: Conf. Ser. **200**, 012004 (2010).

[8] T. Ali, E. Bauer, G. Hilscher, and H. Michor, Phys. Rev. B **83**, 115131 (2011).

[9] T. Kohara, T. Oda, K. Ueda, Y. Yamada, A. Mahajan, K. Elankumaran, Z. Hossian, L. C. Gupta, R. Nagarajan, R. Vijayaraghavan, and C. Mazumdar, Phys. Rev. B **51**, 3985 (1995).

[10] M. E. Hanson, F. Lefloch, W. H. Wong, W. G. Clark, M. D. Lan, C. C. Hoellwarth, P. Klavins, and R. N. Shelton, Phys. Rev. B **51**, 674 (1995).

[11] B. J. Suh, F. Borsa, D. R. Torgeson, B. K. Cho, P. C. Canfield, D. C. Johnston, J. Y. Rhee, and B. N. Harmon, Phys. Rev. B **54**, 15341 (1996).

[12] B. J. Suh, F. Borsa, D. R. Torgeson, B. K. Cho, P. C. Canfield, D. C. Johnston, J. Y. Rhee, and B. N. Harmon, Phys. Rev. B **53**, R6022 (1996).

[13] P. Blaha, K. Schwarz, G. Madsen, D. Kvasnicka, and J. Luitz, "Wien2k", tU-Wien, http://www.wien2k.at/index.html (2011).

[14] T. Ali, S. Manalo, H. Michor, C. Ritter, D. Reith, and R. Podloucky (unpublished).

[15] J. P. Perdew, K. Burke, and M. Ernzerhof, Phys. Rev. Lett. **77**, 3865 (1996).

[16] P. Haas, F. Tran, and P. Blaha, Phys. Rev. B **79**, 085104 (2009).

[17] P. Blaha, K. Schwarz, and P. Herzig, Phys. Rev. Lett. **54**, 1192 (1985).

[18] M. Winter, the University of Sheffield, http://www.webelements.com (2011).

[19] P. Novák, F. Boucher, P. Gressier, P. Blaha, and K. Schwarz, Phys. Rev. B **63**, 235114 (2001).

[20] D. J. Singh and W. E. Pickett, Phys. Rev. B **51**, 8668 (1995).

[21] L. F. Mattheiss, Solid State Commun. **94**, 741 (1995).

[22] Materials Preparation Center, Ames Laboratory, US DOE Basic Energy Sciences, Ames, IA, USA, http://www.mpc.ameslab.gov (2012).

[23] N. W. Ashcroft and N. D.Mermin, in *Solid State Physics*, Chap. 31 (Holt-Saunders International Editions, London, 1976), p. 669.

[24] T. Ali, Ph.D. dissertation, Technical University, Vienna, Austria, 2011.

[25] G. C. Carter, L. H. Bennett, and D. J. Kahan, *Metallic Shifts in NMR, Pt. I* (Pergamon, New York, 1977).

[26] S. Blügel, H. Akai, R. Zeller, and P. H. Dederichs, Phys. Rev. B **35**, 3271 (1987).

[27] A. Narath, Phys. Rev. **162**, 320 (1967).

[28] T. Moriya, *Spin Fluctuations in Itinerant Electron Magnetism*, Solid-State Sciences, Vol. 56 (Springer, Berlin, 1985).

[29] D. E. MacLaughlin, M. Daugherty, and K. Parvin, Solid State Commun. **12**, 5 (1973).

[30] H. Y. Carr and E. M. Purcell, Phys. Rev. **94**, 630 (1954).